Monthly Notices of the ROYAL ASTRONOMICAL SOCIETY

MNRAS **510,** 5302–5314 (2022) https://doi.org/10.1093/mnras/stab3761
Advance Access publication 2021 December 27

Detection of ^{7}Be II in the Small Magellanic Cloud

Luca Izzo [1★] Paolo Molaro [2,3★] Gabriele Cescutti [2,3,4] Elias Aydi [5] Pierluigi Selvelli,[2] Eamonn Harvey [6] Adriano Agnello,[1] Piercarlo Bonifacio [7] Massimo Della Valle [8,9] Ernesto Guido[10] and Margarita Hernanz [11]

[1]*DARK, Niels Bohr Institute, University of Copenhagen, Jagtvej 128, DK-2200 Copenhagen, Denmark*
[2]*INAF, Osservatorio Astronomico di Trieste, Via Tiepolo 11, I-34143 Trieste, Italy*
[3]*IFPU, Istitute for the Fundamental Physics of the Universe, Via Beirut, 2, I-34151 Grignano, Trieste, Italy*
[4]*INFN, Sezione di Trieste, Via A. Valerio 2, I-34127 Trieste, Italy*
[5]*Center for Data Intensive and Time Domain Astronomy, Department of Physics and Astronomy, Michigan State University, East Lansing, MI 48824, USA*
[6]*Astrophysics Research Institute, Liverpool John Moores University, IC2 Liverpool Science Park, Liverpool L3 5RF, UK*
[7]*GEPI, Observatoire de Paris, Université PSL, CNRS, Place Jules Janssen, F-92195 Meudon, France*
[8]*Capodimonte Astronomical Observatory, INAF-Napoli, Salita Moiariello 16, I-80131, Napoli, Italy*
[9]*ICRANet, Piazza della Repubblica 10, I-65122 Pescara, Italy*
[10]*Telescope Live, Spaceflux Ltd, 71-75 Shelton Street, Covent Garden, London WC2H 9JQ, UK*
[11]*Institute of Space Sciences (ICE, CSIC) and IEEC, Campus UAB, Camí de Can Magrans s/n, E-08193 Cerdanyola del Valles (Barcelona), Spain*

Accepted 2021 December 21. Received 2021 December 19; in original form 2021 November 6

ABSTRACT

We analyse high-resolution spectra of two classical novae that exploded in the Small Magellanic Cloud (SMC). ^{7}Be II resonance transitions are detected in both ASASSN-19qv and ASASSN-20ni novae. This is the first detection outside the Galaxy and confirms that thermo-nuclear runaway reactions, leading to the ^{7}Be formation, are effective also in the low-metallicity regime, characteristic of the SMC. Derived yields are of N(^{7}Be = ^{7}Li)/N(H) $= (5.3 \pm 0.2) \times 10^{-6}$ which are a factor 4 lower than the typical values of the Galaxy. Inspection of two historical novae in the Large Magellanic Cloud observed with *IUE* in 1991 and 1992 showed also the possible presence of ^{7}Be and similar yields. For an ejecta of $M_{H,\,ej} = 10^{-5}$ M$_\odot$, the amount of ^{7}Li produced is of $M_{^7Li} = (3.7 \pm 0.6) \times 10^{-10}$ M$_\odot$ per nova event. Detailed chemical evolutionary model for the SMC shows that novae could have made an amount of lithium in the SMC corresponding to a fractional abundance of A(Li) $\approx$ 2.6. Therefore, it is argued that a comparison with the abundance of Li in the SMC, as measured by its interstellar medium, could effectively constrain the amount of the initial abundance of primordial Li, which is currently controversial.

Key words: nuclear reactions, nucleosynthesis, abundances – stars: individual: ASSASN-19qv, ASASSN-20ni – (stars:) novae – Galaxy: abundances – Galaxy: evolution.

1 INTRODUCTION

Lithium is the only *metal* element produced during the Big Bang nucleosynthesis (BBN) due to the lack of stable nuclei with mass number eight (Fields, Molaro & Sarkar 2014). The element abundances predicted by the standard BBN theory for the baryonic density coming from the *Planck* mission agree well with those observed, except for ^{7}Li (Fields 2011; Coc, Uzan & Vangioni 2014). Indeed, the abundance of lithium measured in the low-metallicity Galactic halo stars is A(^{7}Li) = log[N(^{7}Li)/N(H)] + 12 = 2.25 (Spite & Spite 1982; Sbordone et al. 2010; Bonifacio et al. 2015), which is $\sim$3 times below the estimate of the standard cosmological model $A(^7\mathrm{Li}) = 2.72 \pm 0.06$ (Cyburt et al. 2016). The latter value depends on the baryon-to-photons ratio $\eta = \frac{N_b}{N_\gamma} \propto \Omega_B h^2$, with Ω_b is the cosmological baryon density and h is the dimensionless hubble parameter (Planck Collaboration XIII 2016). This problem is also known as the *Cosmological Lithium problem* (Fields et al. 2014). A possible solution can be ascribed to convective diffusion in the pre-main-sequence phase as well as during the lifetime of these halo stars (Fu et al. 2015) or to new physics beyond the standard model. On the other hand, the young stellar populations in our Galaxy show Li-abundances four times greater than the SBBN estimate and more than one order of magnitude greater than the halo stars (Spite 1990; Lambert & Reddy 2004; Lodders, Palme & Gail 2009; Ramírez et al. 2012; Fu et al. 2018). The evidence of a growth requires the existence of additional lithium factories. In the last decades several astrophysical Li sources have been proposed, like Galactic cosmic-rays, AGB stars, low-mass Carbon stars, type II supernovae, and classical novae (D'Antona & Matteucci 1991; Romano et al. 1999; Prantzos 2012; Matteucci 2021). The recent detection in the outburst spectra of classical novae of ^{7}Li and ^{7}Be II, an isotope whose unique decay channel is into lithium through electron capture, have confirmed these objects as Li producers. The corresponding yields inferred have placed nova explosions as the main lithium factories in the Galaxy. The time-scales involved also match, as shown by

★ E-mail: luca.izzo@nbi.ku.dk (LI); paolo.molaro@inaf.it (PM)

detailed Galactic chemical evolution (Izzo et al. 2015; Tajitsu et al. 2015; Molaro et al. 2016; Izzo et al. 2018; Cescutti & Molaro 2019; Grisoni et al. 2019; Molaro et al. 2020a; Matteucci 2021).

Classical novae (CNe) are stellar explosions originating from a white dwarf that accretes matter from a late-type main sequence, or in some cases a red giant companion (Bode & Evans 2012). The matter accreted on to the white dwarf surface piles up leading to an increase of pressure and temperature until CNO thermo-nuclear reactions ignite (Gallagher & Starrfield 1978) that leads to an explosive ejection of the accreted layers into the interstellar medium (Gehrz et al. 1998). During this thermo-nuclear runaway process (TNR; Starrfield et al. 1978), we witness the formation of the ^{7}Be isotope through the ^{3}He(α, γ)^{7}Be process. The synthesized beryllium decays into lithium through electron-capture with a half-lifetime decay of ∼53 d (Cameron & Fowler 1971). Given that ^{7}Li is very easily destroyed in almost every astrophysical process, ^{7}Be has to be transported to zones that are cooler than those where it was formed, with a time-scale shorter than its decay time, in order to be detected. This beryllium transport mechanism, as first suggested by Cameron (1955), requires a dynamic situation that is encountered so far only in asymptotic giant branch (AGB) stars and novae.

With an absolute magnitude at maximum that ranges between $V = -10$ mag and $V = -6$ mag (Della Valle & Izzo 2020), CNe can be observed also in nearby galaxies, in particular in the nearby Magellanic clouds. These two Milky Way galaxy satellites are characterized by a low metallicity [$\sim$0.5 $Z_\odot$ for the Large Magellanic Cloud (LMC) and $\sim$0.2 $Z_\odot$ for the Small Magellanic Cloud (SMC); Madden et al. 2013]. Only in recent years, thanks to high-resolution spectrographs mounted at large telescopes, it was possible to detect the very weak interstellar line of ^{7}Li λ 670.8 nm towards a star belonging to the SMC (Howk et al. 2012). The measurement of its abundance, $A(^7\mathrm{Li}) = 2.68 \pm 0.16$ taken at face value is very close with the predictions from the standard BBN, $A(^7\mathrm{Li}) = 2.72 \pm 0.06$ (Cyburt et al. 2016).

Following the detection of ^{7}Be in the ejecta of several classical Galactic novae (Tajitsu et al. 2015; Molaro et al. 2016; Izzo et al. 2018; Molaro et al. 2020a), we report here the attempts to observe this isotope in extragalactic classical novae. After the 2016 outburst of the SMC Nova 2016-10a, also known as MASTER OT J010603.18-744715.8 (Aydi et al. 2018), we had to wait until 2019 July 4 to observe another bright nova in the SMC, ASASSN-19qv (SMCN-2019-07a), and one more year to observe ASASSN-20ni (AT2020yeq). In this work, we present the first extragalactic ^{7}Be II detection in high-resolution spectral observations of the novae ASASSN-19qv and ASASSN-20ni. The implications for the chemical evolution of lithium in the SMC are then discussed.

2 OBSERVATIONS

2.1 ASASSN-19qv

The classical nova ASASSSN-19qv was discovered by the ASAS-SN survey (Shappee et al. 2014; Kochanek et al. 2017) on 2019 July 4 as a new transient of $g = 14.2$ mag in the direction of the SMC as shown in Fig. 1. There is a source in the *Gaia* DR2 (ID 4685624636344633728) at the position of the nova for which the reported parallax is negative, suggesting a very distant object, in agreement with being as distant as the SMC. The *Gaia G* magnitude for this source is $G = 20.68$ mag. The field of view of ASASSN-19qv was observed by the SMASH survey (Nidever et al. 2017) in the *ugriz* filters. There is a source at the position of ASASSN-19qv in all the filter images, which is slightly extended towards the NE

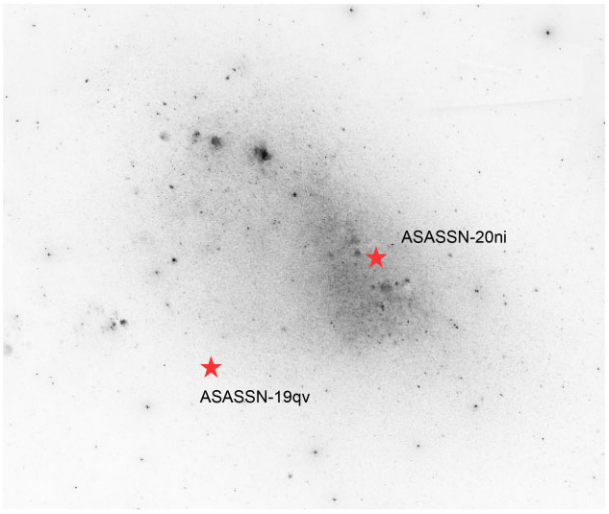

Figure 1. The DSS2 image of the SMC obtained by the Anglo-Australian Observatory (AAO) with the UK Schmidt Telescope. The positions of the two novae are marked with a red star.

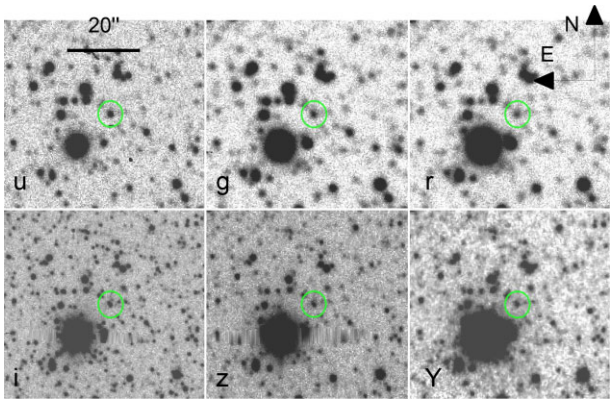

Figure 2 Multi-images of the field of view around ASASSN-19qv as observed in the *ugriz*-bands by the SMASH survey (Nidever et al. 2017) and in the *Y* band as observed by the VISTA Magellanic Cloud survey (Cioni et al. 2011). The position of the nova is marked with a green circle and it shows the counterpart reported in the text.

direction, suggesting that this source is actually composed by two stars. Using nearby stars taken from the USNO B1 catalogue, we measure a magnitude for this source of $i = 20.0 \pm 0.5$ mag. We have also found a catalogue photographic magnitude of $B_j = 20.65$ in the Guide Star Catalog release 2.3 (Bucciarelli et al. 2008) for the source reported at the position of the nova. Additionally, the field of view of ASASSN-19qv was covered by the VISTA Magellanic Cloud survey (Cioni et al. 2011) on 2014 August 16. One source in the *Y* band is coincident with the position reported for ASASSN-19qv (see Fig. 2) for which we determine $Y = 21.3$ mag. However, the double nature of the SMASH source suggests that it could be a foreground faint Galactic star or possibly red giant in the SMC. High-resolution imaging combined with spectroscopic observations of this source during the quiescence phase will definitely reveal the real nature of the progenitor.

A first spectrum obtained 2 d after the discovery of the nova confirmed the transient as a classical nova thanks to the identification of P-Cygni lines of Fe II, O I, and Na I in addition to Balmer lines, with expanding blue-shifted velocities of $\sim -900, -1000$ km s^{-1} (Aydi

Table 1. Log of the observations.

Epoch (d)	Instrument	Exp. time (s)	Wav. range (nm)	Resolution R ($\lambda/\delta\lambda$)
		ASASSN-19qv		
2	Goodman	1 x 500	400–800	∼1850
16	UVES	3 x 900 and 3 x 300	310–945	40 000
29	X-shooter	2 x 600 and 2 x 300	300–2500	6700–8900
81	X-shooter	2 x 600 and 2 x 300	300–2500	6700–8900
		ASASSN-20ni		
4	UVES	1 x 1800 and 3 x 900	310–945	40 000
17	UVES	2 x 600	380–945	40 000
20	UVES	1 x 2200 and 2 x 600	310–945	40 000
29	UVES	1 x 2200 and 3 x 600	310–945	40 000
40	UVES	1 x 1800 and 2 x 900	310–945	40 000

et al. 2019). Spectroscopic observations obtained in the following days (Days 5 and 8; Bohlsen 2019a, b) still showed the presence of Fe II absorption lines and the absence of higher ionization transition like He I. We started to observe ASASSN-19qv with the UVES spectrograph at ESO Very Large Telescope (Program ID: 2103.D-5044, PI Izzo) after 16 d from discovery. The wavelength range covered by UVES starts from 310 to 950 nm at a spectral resolution of $R = 40000$. The following two epochs, Day 29 and Day 81, were obtained with X-shooter at ESO/VLT, covering a wider spectral range from 300 to 2500 nm and with a resolution variable from $R = 6700$ for the VIS and NIR arms to $R = 8900$ for the UVB arm. The detailed log of the observations is shown in Table 1.

2.2 ASASSN-20ni

ASASSN-20ni was also discovered by the ASAS-SN survey on 2020 October 26 as a new transient of $g \sim 14.1$ mag and was confirmed the following day when it increased in brightness to $g \sim 12.2$ mag (Way et al. 2020). The ASAS-SN survey also monitored the position of the sky where ASASSN-20ni was located in the previous 6 yr, and no previous outburst from the nova progenitor brighter than $g > 16.5$ mag were reported.

We searched for the possible presence of the nova progenitor in archival data surveys. To improve the astrometry from ASAS-SN we used the UVES acquisition image to calibrate astrometry at sub-arcsecond precision. No clear sources have been found in the SMASH survey and in the VISTA Magellanic Cloud survey down to a magnitude limit of $Y > 21.5$ mag, despite the nova being 2 arcsec from a bright ($Y = 17.8$ mag) star and 1.5 arcsec from another fainter source see also Fig. 3.

The day following the discovery ASASSN-20ni was classified as a Fe II nova using the Goodman spectrograph covering the wavelength range between 620 and 720 nm (Aydi et al. 2020). The spectrum was characterized by P-Cygni emission-line profiles for Balmer, Fe, and N lines with absorption trough minimum at $v_{\rm exp} \sim -500$ km s^{-1}. We started to observe ASASSN-20ni with the UVES spectrograph using a dedicated Discretional Director Time program [Program ID: 2106.D-5008(B), PI Izzo] 4 d after the nova discovery. We used different exposure times for the different UVES arms and dichroic configurations, in order to optimize the signal-to-noise in the near-UV range and at the same time avoid possible saturation from bright lines between 480 and 850 nm. The log of the observations is shown in Table 1.

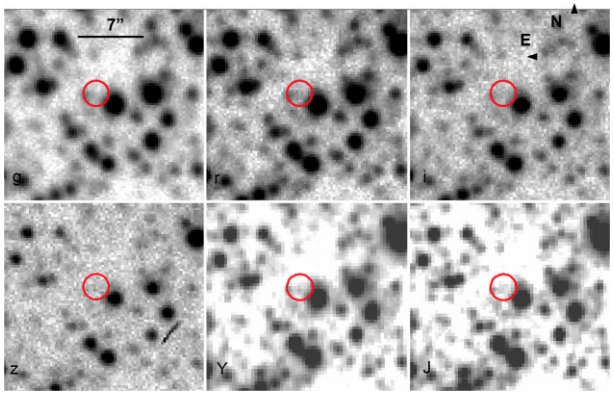

Figure 3 Multi-images of the field of view around ASASSN-20ni as observed in the *griz*-bands by the SMASH survey (Nidever et al. 2017) and in the *YJ*-bands as observed by the VISTA Magellanic Cloud survey (Cioni et al. 2011). The position of the nova calibrated with the UVES acquisition image is marked with a red circle

For both novae, we reduced the UVES and X-Shooter data using a pre-compiled pipeline based on the *python-cpl* libraries, which make use of the standard ESO Recipe Execution Tool (*esorex*).

3 DATA ANALYSIS

3.1 ASASSN-19qv

The light curve of ASASSN-19qv was obtained using AAVSO (Kafka 2021) data and TESS public data.[1] TESS data cover the range between 600 and 1000 nm with a very high temporal sampling. At a cadence of 0.5 h cadence, they reveal presence of fluctuations with amplitude of 0.1–0.2 mag on a time-scale of a few hours (see Fig. 4). There is a lack of data after ∼60 d from the nova discovery. The V-band early evolution is well modelled as an exponential decay with constant decay $b = 0.05$ mag d^{-1}. The best fit with such a function provides also an estimate for the t_2 value, which results to be $t_2 = 11.0$ d, implying that ASASSN-19qv is close to being classified as a fast nova, according to the classification of Payne-Gaposchkin (1957).

The high-resolution spectrum provided by UVES allows us to identify SMC interstellar lines, like Ca II H,K lines, and then to determine the velocity offset due to the motion of the SMC that will be considered in the analysis presented in this work. In Fig. 5, we show the heliocentric radial velocity of both Ca II IS lines, in addition to the Na I D2 line. While Na I is almost absent in the SMC environment, the Ca II lines are clearly detected and they are characterized by a main absorption centred at $v_{\rm SMC,\,1} = 130$ km s^{-1}, which will be considered as the main SMC offset in the rest of the analysis for this nova. We also note a narrow component at lower velocities, $v_{\rm SMC,\,2} = 90$ km s^{-1} likely due to an additional cloud of interstellar gas in the SMC along our line of sight.

3.1.1 The spectroscopic evolution

Our first spectrum covers the 400 – 800 nm range and was observed only 2 d after discovery. It is characterized by the presence of Balmer, Na I and Fe II P-Cygni absorption lines with blue-shifted absorption velocities between −900 and −1000 km s^{-1}. The O I λ777.5 nm

[1] https://heasarc.gsfc.nasa.gov/docs/tess/

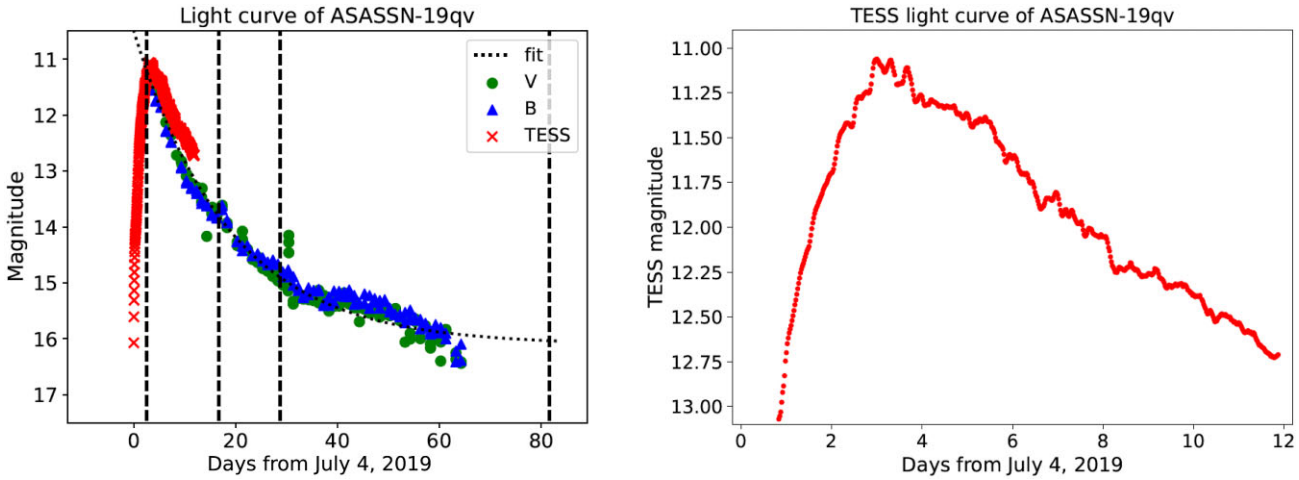

Figure 4 Left-hand panel: The light curve of ASASSN-19qv as obtained from the AAVSO data archive (Kafka 2021) in the *B* and *V* filters and using the early TESS data, as described in the text. Dashed lines correspond to the spectral epochs presented in this work. The dotted curve represents the best fit that we have found using an exponential decay function. Right-hand panel: An in-depth view of TESS data. The light curve shows small fluctuations in magnitude with amplitude of 0.1–0.2 mag.

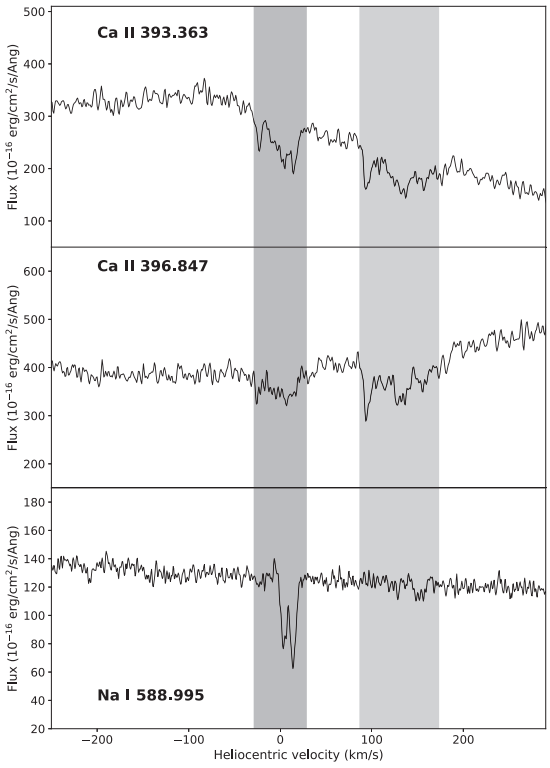

Figure 5. The Day 16 spectrum of ASASSN-19qv centred around the Ca II λ393.3 (upper panel), the Ca II λ396.8 lines (middle panel), and around the Na I λ588.995 nm IS line (lower panel). Velocities are corrected for the heliocentric correction. The SMC interstellar Ca II absorptions are observed at $v_{\rm SMC} = +130$ km s^{-1} and are broader than the corresponding Milky Way (MW) lines. These are marked with a light grey strip, while the MW component is reported with a darker strip.

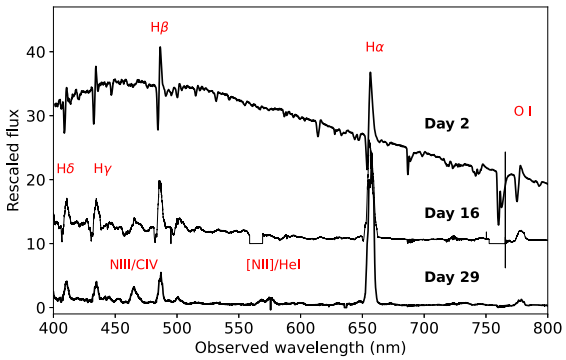

Figure 6. Spectral evolution of the nova ASASSN-19qv in the first month after the discovery. Spectra have been rescaled in flux and shown in the range (400, 800) nm. The presence of helium, blended with Fe II, nitrogen lines and of a bright Bowen blend at 464.0 nm observed in the Day 16 spectrum marks the transition from the Fe II to the He/N type, classifying this nova as a hybrid case, according to Williams (1994). In the Day 29 spectrum, the presence of a rising [N II] 575.5 nm line marks the transition to the 'auroral' phase.

line is the brightest non-Balmer line, implying that this spectrum is typical of the Fe II nova spectral class (see also Fig. 6).

The second spectrum obtained 16 d after the nova discovery peaks at bluer wavelengths than the first spectrum. It shows P-Cygni profiles for Balmer lines characterized by two main absorption components, at the blue-shifted velocities of $v_{1,a} = -1710$ km s^{-1} and $v_{1,b} = -2400$ km s^{-1}. The brightest non-Balmer line is O I λ844.6 nm. The Fe II λ516.9 nm line now shows fainter P-Cygni absorptions at the same velocities of the Balmer lines, indicating that the ionization state is increasing. This evidence is also confirmed by the presence of faint, but emerging, He I lines, in particular the He I λ501.6 nm line that is blended with Fe II λ501.8 nm, and the presence of N I and C II lines. The third spectrum (Day 29) shows higher ionization transitions like the Bowen (N III–C IV) blend at 464.0 nm in addition to a rising [N II] λ575.5 nm line, which mark the beginning of the 'auroral' phase. In the near-IR range the brightest line, with the exception for the Paschen-α, is O I λ1128.7 nm as it is expected given the high luminosity of the O I λ844.6 nm line. This evidence suggests that the photo-excitation by accidental resonance (Kastner & Bhatia 1995) is still working at this epoch. The ratio $R_{{\rm O}i}$ between O I λ844.6 nm / O I λ777.5 nm has been proposed by Williams (2012) as a density diagnostic for the ejecta. We measure

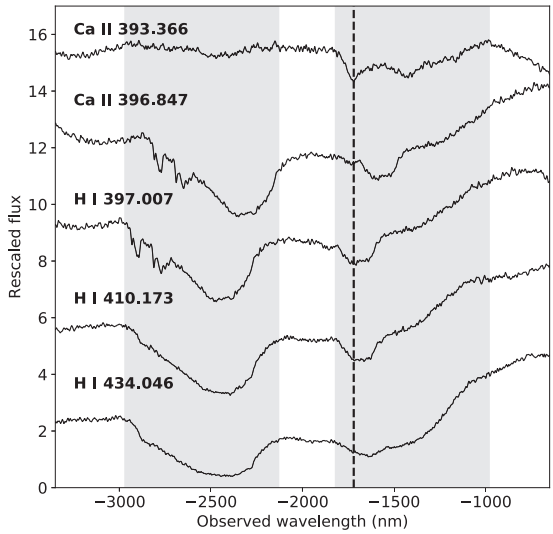

Figure 7. Day 16 spectrum of ASASSN-19qv, corrected for the SMC motion, showing the P-Cygni absorptions of Ca II H,K lines and Balmer H γ, H δ, and H ϵ lines. The absorption components are clearly visible in all Balmer lines. The Ca II 396.847 nm is blended in the broad P-Cygni of Hϵ and only the prominent feature at $v = -1720$ km s^{-1} is clearly visible (the dashed black line). The high-velocity component in the Ca II 393.366 nm line is less pronounced, suggesting a very low density for the Calcium in this component.

$R_{\mathrm{O}i,1} = 3.5$ in the Day 14 spectrum and $R_{\mathrm{O}i,1} = 12.6$ in the Day 29 spectrum, suggesting a relatively high density of the ejecta, more similar to Fe II-type novae, but rapidly decreasing between the two epochs.

The wavelength range of the spectra obtained with UVES and X-shooter extends to the near-UV part of the electromagnetic spectrum, permitting to analyse with a good signal-to-noise ratio the region where the resonance transition of the ^{7}Be II λ 313.0/1 nm doublet isotope falls. Indeed, in both early epochs (Day 14 and Day 29), we detect blue-shifted absorption components that we have identified as due to the ^{7}Be II λ 313.0/1 nm transition (see also Figs 7 and 8). In the Day 14 spectrum, we clearly see two broad P-Cygni absorptions that share the same expanding velocities of the P-Cygni absorptions observed in Balmer lines, as well as in other transition as O I. These absorption components are characterized by expanding velocities of $v_{\mathrm{Day16,\,1}} = -1630$ km s^{-1} and $v_{\mathrm{Day16,\,2}} = -2400$ km s^{-1} as observed in the Day 14 spectrum, with the slow component being less intense than the fast one. This difference is more clear in the spectrum obtained on Day 29, where the slow expanding component, with a measured velocity of $v_{Day29,\,1} = -1790$ km s^{-1}, becomes more narrow while the fast component is characterized by a broad profile (FWHM$_{\mathrm{H}\,\beta}$ $\approx$ 900 km s^{-1}) centred at the value of $v_{\mathrm{Day29,\,2}} = -2600$ km s^{-1}. This behaviour is observed in all the main Balmer lines as well as in the ^{7}Be II λ 313.0/1 nm transition. This is the main evidence that beryllium was synthesized during the TNR preceding the outburst of ASASSN-19qv.

The Day 81 spectrum shows the absence of high-velocity blue-shifted absorption features, observed in the previous epochs, but we still detect permitted transitions like O I 844.6 nm (including the 1129.1 nm in the near-IR range), and the flux ratio with the O I 777.5 nm which is blended with [Ar III] is now $R_{\mathrm{O\,I}} = 8.1$, suggesting an environment still relatively dense. There are also high-ionization lines such as He I ground state transitions 1008.3/2005.8 nm as well as excited transitions (587.6/706.5 nm lines among the many others barely discernible in the spectrum). We also detect the presence

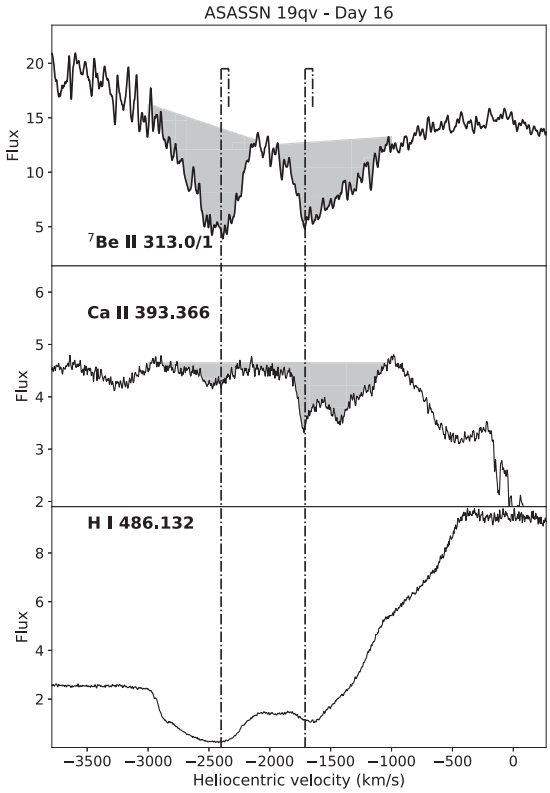

Figure 8 The Day 16 spectrum of ASASSN-19qv, corrected for the SMC motion, showing the P-Cygni absorptions of the ^{7}Be II λ313.0 at blue-shifted velocities of $v_{1a} = -1710$ km s^{-1} and $v_{1b} = -2400$ km s^{-1} and compared with the Ca II λ396.8 and with H β. The dashed regions mark the area of the absorptions considered for the EW estimate.

of typical forbidden transitions observed in the nebular phase of classical novae like the [O III] 436.3/495.9/500.7 nm, the [N II] 575.5 nm, suggesting that the physical conditions of the ejecta at this stage are very heterogeneous. Then we cannot use this spectrum to infer physical properties like the density, temperature, and the hydrogen mass of the ejecta. We do not detect forbidden neon lines at this epoch, suggesting a CO-type WD for the nova progenitor.

3.2 ASASSN-20ni

The light curve of ASASSN-20ni was built using AAVSO data (Kafka 2021). We have also used ASAS-SN *g*-band data that covers the rising phase of the nova and its decay up to ~60 d after the peak brightness (see Fig. 10). The last non-detection from the ASAS-SN survey was dated 2020 October 25, e.g. one day before the first nova detection by the same project (Way et al. 2020). The light-curve evolution in the first 60 d of the nova emission can be modelled using an exponential function, despite the light curve showing a short re-brightening at ~20 d from the peak brightness. Using the AAVSO *V*-band data, we measure a decay rate of $b = 0.02$ mag d^{-1}, and a t_2 parameter of $t_2 = 17.4$ d, which classify ASASSN-20ni as a fast nova.

ASASSN-20ni was observed in the central region of the SMC, whereas ASASSN-19qv was located at a more peripheral region (see Fig. 1). This is reflected on the amount of gas surrounding the nova location as inferred from the analysis of interstellar lines. As

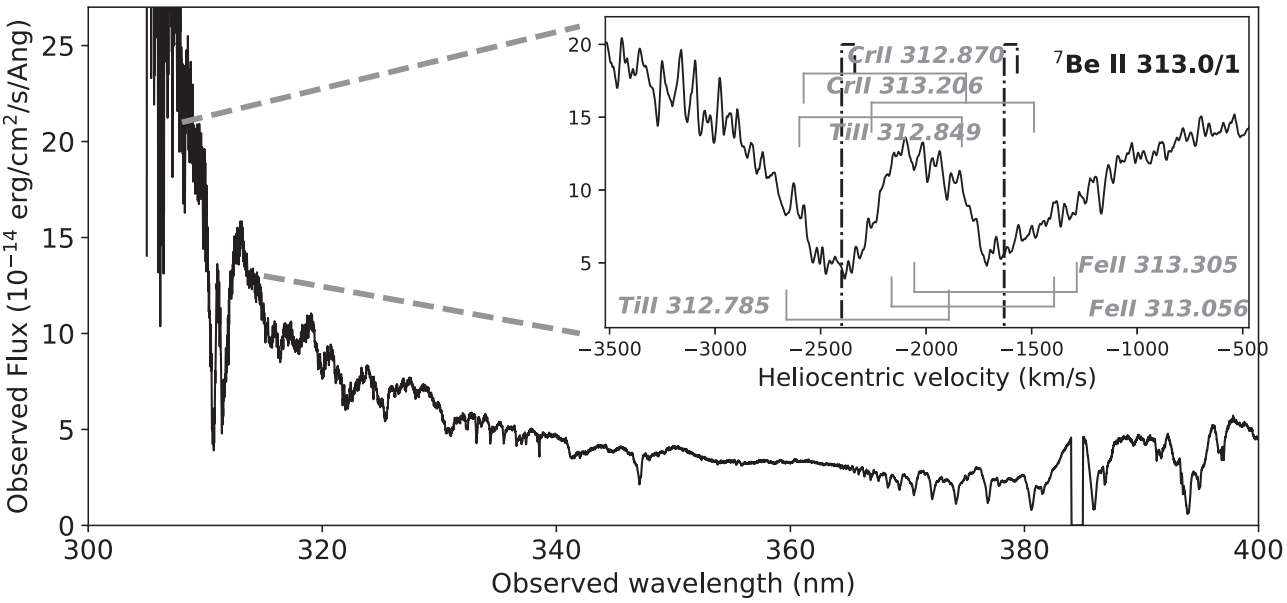

Figure 9 The Day 16 spectrum of ASASSN-19qv in the region 300–400 nm. The inset plot shows the region centred around the Be II λ313.058, which shows the expected positions of low ionization transition absorptions of Cr II, Ti II, and Fe II. Velocities are corrected for the heliocentric correction.

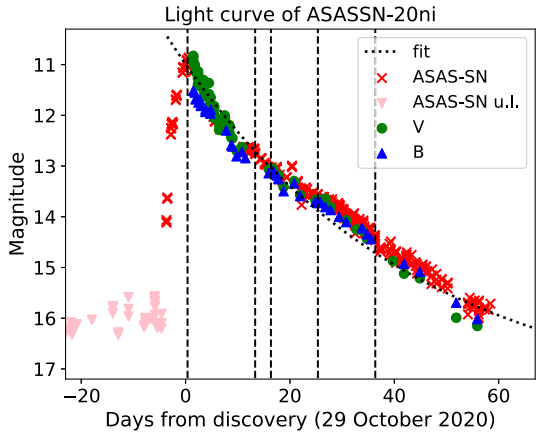

Figure 10 The light curve of ASASSN-20ni as obtained from the AAVSO data archive (Kafka 2021) in the *B* and *V* filters and using the ASAS-sn *g* filter data, as described in the text. Dashed lines correspond to the spectral epochs presented in this work. The dotted curve represents the best fitting found using an exponential decay function.

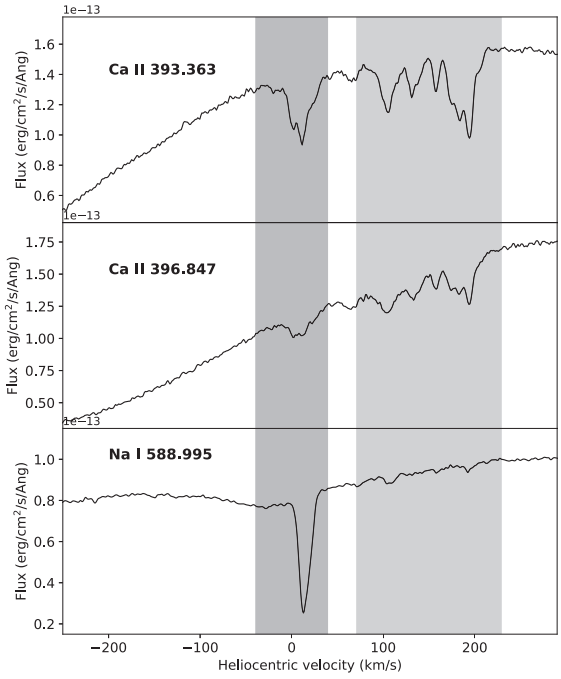

Figure 11. The Day 4 spectrum of ASASSN-20ni centred around the Ca II λ393.3 (upper panel), the Ca II λ396.8 lines (middle panel), and around the Na I λ588.995 nm IS line (lower panel). Velocities are corrected for the heliocentric correction. The SMC interstellar Ca II absorptions are observed at multiple velocity (see the text).

observed in the Ca II H,K lines, we note multiple components at $v_{\rm SMC}$ = 105, 131, 156, and 194 km s^{-1}, with the latter being the most intense component (see also Fig. 11). Similar to the spectrum of ASASSN-19qv, the Na I interstellar component is less pronounced, showing only the components at $v_{\rm SMC}$ = 105 and 194 km s^{-1}. In the following, we will consider the highest velocity component at $v_{\rm SMC}$ = 194 km s^{-1} as our reference to correct all our spectral series to the SMC velocity.

3.2.1 *The spectroscopic evolution*

The first spectrum of ASASSN-20ni was obtained just 4 d after its discovery. It shows a very optically thick continuum, typical of the Fe II spectral class (Williams et al. 1991), and is characterized by the presence of a 'forest' of absorption lines in the range between 300 and 550 nm (see also Fig. 12). After re-scaling the spectrum at the SMC velocity assumed for this nova, we measure blue-shifted absorption velocities of $v_{exp} \sim -520$ km s^{-1} for Na I, Ca II, and Fe II lines, while Balmer lines show a broader absorption trough extending to higher velocities. We also detect at the same expanding velocity the majority of THEA lines listed in table 2 of Williams et al. (2008), with the exception of V II lines. We cannot clearly confirm the

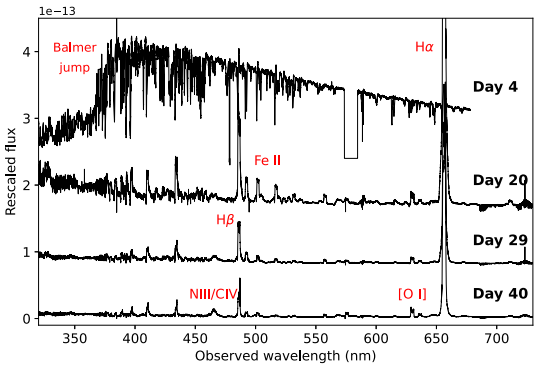

Figure 12. Spectral evolution of the nova ASASSN-19qv in the first 40 d after the discovery. Spectra have been rescaled in flux and shown in the range (330, 740) nm.

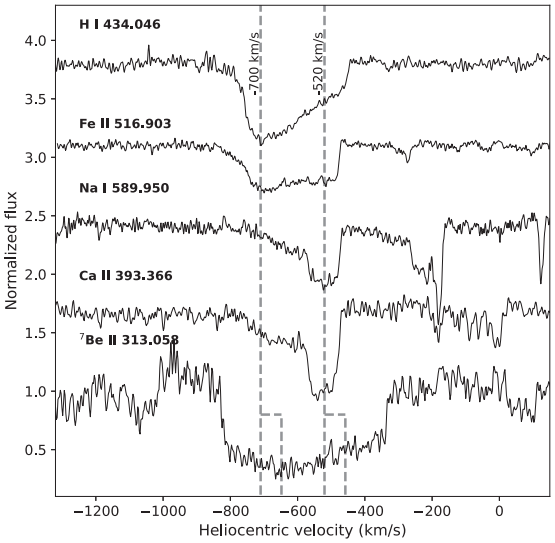

Figure 13. The Day 40 spectrum of ASASSN-20ni, corrected for the SMC motion, showing the P-Cygni absorptions of Ca II K, H γ, Fe II 516.9 nm, Na I 589.9 nm and of ^{7}Be II 313.0 nm lines. The plot shows the different profile of Ca II and Na I, which show a prominent absorption at -530 km s^{-1} and a more faint high-velocity tail, with respect to H I, Fe II, and ^{7}Be II lines, where the higher velocity component centred at ~ -700 km s^{-1} and extending to -800 km s^{-1} is more pronounced. This evidence suggests a different abundance composition for the two components and supports a two-ejecta component scenario (Mukai & Sokoloski 2019). For the ^{7}Be II line are reported the expected positions of the two doublet components.

presence of Li I 670.7nm, despite broad absorption being observed at the corresponding blue-shifted wavelength.

The second spectrum, obtained two weeks later (Day 17), and covering the range from 375 to 500 nm and from 580 to 946 nm, shows an evolved spectrum where almost all THEA lines have disappeared. The brightest non-Balmer line is O I 844.6 nm, showing a main P-Cygni absorption system at higher velocities $v_{exp} = -700$ km s^{-1}, similar to what is measured for Balmer and Fe II lines. Interestingly, the Na I doublet shows a more structured profile, with signatures of two components at velocities of $v_1 = -650$ km s^{-1} and $v_2 = -520$ km s^{-1}. This velocity configuration for the ejecta is also observed in the following spectra (Day 20 and Day 29). At these epochs, bright emission lines display a saddle-shaped profile with the two bright peaks at $\pm\sim$500 km s^{-1}, which suggests an asymmetric geometry for the nova ejecta (Mukai & Sokoloski 2019). The last spectrum obtained on Day 40 still presents low-ionization transitions such as the Fe II multiplet 42, but we also see enhanced higher ionization transitions such as the Bowen blend in emission and the He I 587.5 nm, which was identified by the presence of a P-Cygni absorption with blue-shifted velocity of ~ -650 km s^{-1}. Interestingly, lower ionization transitions such as Ca II, Fe II, and Na I show a more intense lower velocity (~ -520 km s^{-1}) component overimposed to the higher velocity component with intensity fading with the increasing velocity to -700 km s^{-1} (see Fig. 13).

4 ABUNDANCE OF ^{7}BE

4.1 ASASSN-19qv

Following Tajitsu et al. (2015), we quantified the amount of beryllium ejected in the ASASSN-19qv outburst by comparing the observed equivalent widths (EW) of the blue-shifted absorption components with the EW of a reference element. The resonance lines of ionized calcium Ca II λλ393.4/396.8 nm H,K are the more suitable, given that calcium shares the same configuration of their outermost electron shells. A detailed analysis of Day 16 spectrum shows the presence of faint blue-shifted components for the Ca II 393.4 nm line centred at the same velocities observed for the Balmer lines (see Fig. 7).

The other doublet component, Ca II 396.8 nm, is blended within the P-Cygni of the H I 397.0 nm line, but we confirm its presence through the identification of a faint feature corresponding to the main absorption observed for all transitions at $v = -1720$ km s^{-1}. Moreover, we observe that the high-velocity absorption components of Calcium lines are much fainter when compared with the slower components, while for ^{7}Be II and Balmer lines this is not observed. This evidence suggests that the high-velocity component ejecta has a distinct element abundance. This difference can be explained in the case that high-velocity components arise from a distinct ejecta event, like the one proposed in Mukai & Sokoloski (2019), where a later fast wind-like, and likely bi-polar ejection is observed after the first phenomenon, which is slower and characterized by an oblated geometrical distribution. We will come back to this point later. In the spectrum obtained on Day 29, Ca II lines almost disappeared. In the Day 29 spectrum, we observed a very faint absorption for Ca II 393.3 nm line (see Fig. 8), and in order to estimate the beryllium abundance we consider the analysis of the UVES Day 16 spectrum.

We have then measured the EWs for the ^{7}Be II and the Ca II 393.4 nm for the blue-shifted absorption area as shown in Fig. 8. However, as also reported in our previous analysis (Molaro et al. 2020a), the absorption of ^{7}Be II is generally contaminated by the presence of low ionization transitions of Cr II, Ti II, and Fe II. We have then analysed the presence of the most intense transitions (see Table 2) that fall close to the wavelength range of ^{7}Be II and in Fig. we report their expected position in the spectral region surrounding the blue-shifted beryllium absorptions. We cannot clearly confirm the presence of Cr II and Ti II, given the relatively low signal-to-noise ratio ($\sim$10) of the UVES spectrum around the ^{7}Be II transitions. We have also checked for the presence of absorption lines from the other transitions of these same elements originating from their parent multiplets, but it is hard to firmly establish their presence. We find possible evidence of the presence of Fe II lines λλ313.305, 313.056, and other transitions arising from the same initial level like Fe II λ316.794, 314.472, whose detection, in addition to the already confirmed presence of Fe II λ516.903, confirms the presence of iron in the ejecta of ASASSN-19qv. Consequently, in our final estimates

Table 2. A list of single-ionized ions which are the main contributors to the absorption in the region around λ313.058 and that are shown in Fig. 9. Atomic data taken from the NIST lines data base. Those for Cr II are from Lawler et al. (2017).

Wavelength (Air) (nm)	Ion	Log(gf)	Low energy (eV)	Upper energy (eV)
312.7850	Ti II	0.15	3.87	7.83
312.8483	Ti II	0.11	3.90	7.87
312.8700	Cr II	−0.53	2.43	6.40
313.0565	Fe II	–	3.77	7.73
313.2057	Cr II	0.43	2.48	6.44
313.3048	Fe II	−1.9	3.89	7.84

of the ^{7}Be II EWs, we are taking into account the presence of these line blends.

Our final results are shown in Table 3, where we report the measured EWs for the low- and high-velocity components, as well as the total value. The EW ratio between ^{7}Be and Ca for low-velocity component, EW(^{7}Be II$_{\rm low}$)/EW(Ca II$_{\rm low}$) $= 2.26 \pm 0.07$, while for the high-velocity component, we measure a much higher value, namely EW(^{7}Be II$_{\rm high}$)/EW(Ca II$_{\rm high}$) $= 8.58 \pm 0.07$. In the following analysis, we will not distinguish between these two emission components, given that both systems are escaping the binary and will then enrich the ISM of the SMC. But, a detailed analysis included in a wider context is needed and will be presented elsewhere. For the entire absorption systems, we consider the average ratio between the two components, obtaining EW(^{7}Be II)/EW(Ca II) $= 3.50 \pm 0.09$. This value slightly exceeds the mean value of $\sim$1.5 ± 0.2 found in Galactic novae (Molaro et al. 2020a). Following Spitzer (1998), the relative number abundance can be inferred from

$$\frac{\rm N(^7Be\ II)}{\rm N(Ca\ II)} = 2.164 \times \frac{\rm EW(^7Be\ II)}{\rm EW(Ca\ II)}. \quad (1)$$

^{7}Be II is unstable with an half-lifetime decay of $t_{1/2} = 53.3$ d. Thus, considering the correction factor of $K = 1.23$ we obtain N(^{7}Be II) $= (9.32 \pm 0.30) \times$ N(Ca II).

4.2 ASASSN-20ni

The velocity distribution of the ejecta along the evolution of the outburst is crucial to identify the presence of features due to the doublet resonance lines of ^{7}Be II. In Fig. 14, the evolution of the region between 310 and 314 nm is shown to highlight the presence of a broad absorption around ∼312.5 nm. This absorption corresponds to ^{7}Be II 313.0/1 nm and matches the blue-shifted velocities reported for other ions observed in the spectrum at the same epoch.

Unfortunately, our spectral observations cover the first 40 d only, such that we could not follow-up the evolution of the ^{7}Be P-Cygni profile until narrow features would appear, as due to the expanding ejecta and its consequent density decay, similar to the case of ASASSN-19qv previously discussed. Moreover, in ASASSN-20ni, we could not disentangle the low- and high-velocity components, being apparently embedded in the observed absorption profile (see Fig. 13). Consequently, we have done a careful measurement of the EW of the total absorption profile, paying attention to the contribution of other lines, such as Fe II, Ti II, and Cr II (see the list in Table 2), similarly to what was done for ASASSN-19qv. The presence of THEA lines in the early spectra of ASASSN-20ni represents important information for our analysis: we already know their expanding velocities that correspond to the lower velocity component, and then their position in the spectrum.

In Table 4, we report on our final measurement of the EW of the ^{7}Be II 313.0/1 nm blue-shifted absorption, as well as of Ca II 393.3 nm, which we will use as our reference for the estimate of the Be abundance, as already discussed in Section 4. The EW ratio between ^{7}Be and Ca is EW(^{7}Be II)/EW(Ca II) $= 2.14 \pm 0.24$, as estimated from the Day 40 spectrum. Assuming a correction factor of $K = 2.11$ for the ^{7}Be II decay, finally we obtain N(^{7}Be II) $= (9.81 \pm 0.52) \times$ N(Ca II), which is in good agreement with the Be abundance value estimated for ASASSN-19qv.

5 DISCUSSION

5.1 ^{7}Be (= ^{7}Li) yields

From our previous analysis, we infer an average beryllium abundance of N(^{7}Be II) $= (9.63 \pm 0.50) \times$ N(Ca II). Following similar studies (Molaro et al. 2022), we assume that singly ionized ions of Be II and Ca II represent the main ionization stage for the ejecta and calcium is not produced in the nova explosion. Calcium can be also synthesized in massive oxygen–neon WDs, where the peak temperatures can reach very high values ($T \sim 5 \times 10^8$ K and more). Some observations have indeed reported Ca abundance values in nova ejecta up to one order of magnitude larger than the Solar value (Andrea, Drechsel & Starrfield 1994), suggesting a possible production channel for heavy ($A \sim 40$) elements in very hot WDs (Christian et al. 2018; Setoodehnia et al. 2018). The lack of neon in ASASSN-19qv suggests that the progenitor WD of ASASSN-19qv is not an extremely, hot massive WD. For ASASSN-20ni, unfortunately, due to the lack of late-time spectra, we could not verify the presence of bright forbidden neon lines in the near-UV, which would imply a ONe underlying WD. However, the larger t_2 value suggests a similar, if not lower, massive WD progenitor. On the other hand, Starrfield et al. (2020) found that a large overproduction of ^{40}Ca (up to ten times the Solar value) is obtained from their 1D hydrodynamic simulations of the TNR in CO novae. An increase in ^{40}Ca abundance would lead to a corresponding increase on the ^{7}Be yield, with important consequences for the lithium enrichment of the SMC. However, measuring ^{40}Ca abundance in nova ejecta requires a high-cadence spectral covergage of the optically thick phases, when the ejecta is relatively cold, given the strong sensitivity of calcium ionization to the ambient temperature (Chugai & Kudryashov 2020; Molaro et al. 2022). We therefore assume here that Ca in the ejecta shares the average value of the SMC stellar populations.

The mean stellar metallicity of the SMC is [Fe/H] $= -0.59 \pm 0.06$, obtained from the analysis of massive and young OB stars (Korn et al. 2000; Bouret et al. 2003; Trundle et al. 2007). Recent measures from a large-scale photometric analysis of the SMC have reported an average value of [Fe/H] $= -0.95 \pm 0.08$, using the slope of the Red Giant branch as an indicator of the metallicity (Choudhury et al. 2018). The location of ASASSN-19qv is, however, quite peripheral, while ASASSN-20ni is in the inner region of the SMC. Carrera et al. (2008) report a significant gradient with the metallicity decreasing towards the external regions. The inner part of the SMC is characterized by higher metallicity values ([Fe/H] ~ -0.6). The existence of two peaks at [Fe/H] $= -0.9/-1.0$ and at [Fe/H] $= -0.6$ in the metallicity distribution of the SMC was also reported in Mucciarelli (2014). In the following, we will use the value of [Fe/H] $= -0.6$ for both novae. Given that the solar abundance of calcium is N(Ca)/N(H)$_\odot$ $= 2.2 \times 10^{-6}$ (Lodders et al. 2009), we obtain that the Ca abundance value in the SMC is N(Ca)/N(H)$_{\rm SMC}$ $= (5.5 \pm 0.4) \times 10^{-7}$. With this

Table 3. Equivalent width measurements for the ^{7}Be II and Ca II 393.4 nm blue-shifted absorptions in the Day 16 spectrum of ASASSN-19qv.

Day	EW(^{7}Be II$_{low}$) (Å)	EW(^{7}Be II$_{high}$) (Å)	EW(^{7}Be II$_{tot}$) (Å)	EW(Ca II$_{low}$) (Å)	EW(Ca II$_{high}$) (Å)	EW(Ca II$_{tot}$) (Å)
16	3.32 ± 0.05	3.09 ± 0.07	6.41 ± 0.09	1.47 ± 0.01	0.36 ± 0.02	1.83 ± 0.02

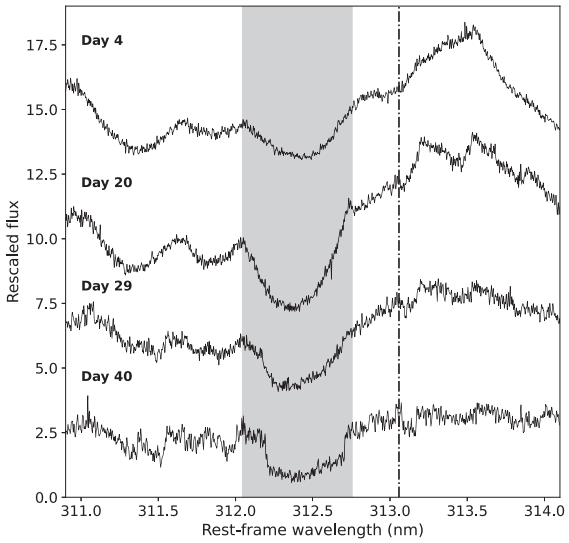

Figure 14. The evolution of the broad absorption feature centred at λ = 312.5 nm, marked with a grey shaded region, and attributed to ^{7}Be II 313.0/1 nm doublet. The dot–dashed black line marks the rest-frame position of the ^{7}Be II 313.0 nm line.

Table 4. Equivalent width measurements for the ^{7}Be II and Ca II 393.4 nm blue-shifted absorptions in the Day 20, 29, and 40 of ASASSN-20ni.

Day	EW(^{7}Be II$_{tot}$) (Å)	EW(Ca II$_{tot}$) (Å)
20	2.45 ± 0.11	2.58 ± 0.11
29	2.19 ± 0.12	2.09 ± 0.13
40	2.77 ± 0.18	1.29 ± 0.12

value we obtain a ^{7}Be, or ^{7}Li yield of N(^{7}Li)/N(H) $= (5.3 \pm 0.2) \times 10^{-6}$.

We are not able to estimate the mass ejected directly but the two novae studied here are fast novae, which suggests high expansion velocities and lighter mass for the ejecta (Warner 1989; Della Valle & Izzo 2020). Uncertainty in the lithium yield is possible when considering that some Calcium could be in the form of Ca III. Chugai & Kudryashov (2020) suggested the possibility that some overionization could be present in the nova ejecta.

This would lead to a decrease in the abundance of Ca II with the consequence to overestimate the total abundance of ^{7}Be. Incidentally, this would alleviate the tension between observations and TNR theory (Starrfield et al. 2020). Molaro et al. (2022), using the photoionization code `Cloudy` (Ferland et al. 2017), showed that overionization in the ejecta of CNe is indeed possible but requires unlikely low densities and high temperatures of the gas. Moreover, the detection of neutral species transitions led them to conclude that the main ionization phase of calcium is the single-ionized stage. We have detected the Mg I 383.8 nm line at the same velocities of the expanding ejecta components of the two novae presented in this work, on Day 16 for ASASSN-190qv and on Day 20 for ASASSN-20ni, respectively. In the spectrum of ASASSN-20ni we also report the presence of Ca I 422.6 nm line, which suggests a low ionization stage for Calcium.

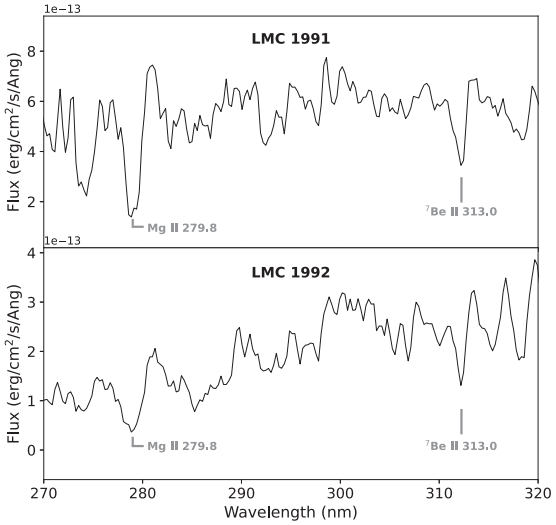

Figure 15. The *IUE* spectra of LMC 1991 (LWP20210LS, 4 d after the nova discovery) and LMC 1992 (LWP24303LL, ∼1 d after the discovery) in the range of 270.0–320.0 nm. The two strong absorption near 279.0 and 312.2 nm are identified as Mg II 280.0 and ^{7}Be II 313.0 at the expanding blue-shifted velocity of $v_{exp} \sim -850$ km s^{-1}, assuming an expanding velocity for the LMC of $v_{\rm LMC} = 240$ km s^{-1} (McConnachie 2012). Both spectra are corrected for reddening using $E(B-V) = 0.15$ mag (see Cassatella, Altamore & González-Riestra 2002).

5.2 Historical novae in the LMC

Following these detections, we searched in the *IUE* archive for observations of classical novae exploded in the Magellanic Clouds with *IUE*, the International Ultraviolet Explorer (Boggess et al. 1978). *IUE* has already been shown suitable for a ^{7}Be search (Selvelli, Molaro & Izzo 2018). The LWP camera of the *IUE* satellite covered the wavelength range of 200.0–320.0 nm and in its low resolution mode, *IUE* ($\Delta\lambda \approx 0.5$ nm), was suitable for checking the presence of a wide feature near 313.0 nm. Nova LMC 1991 and Nova LMC 1992 have been followed by *IUE*. Representative early spectra for these two novae are shown in Fig. 15. Both spectra exhibit a strong absorption feature shortward of λ313.0 nm that can be identified as the blue-shifted resonance doublet of singly ionized ^{7}Be II.

We note that this feature can be only partially explained as a blend of common iron curtain absorption lines of singly ionized metals. Previous studies of galactic novae found only a minor contribution by singly ionized metals, i.e. Cr II, Fe II, and Ti II to this feature (Tajitsu et al. 2015, 2016; Molaro et al. 2016; Selvelli et al. 2018; see also Fig. 9). A blending contribution which is expected to be even lower for Novae in the LMC owing to its low metallicity. Schwarz

et al. (2001), and using PHOENIX model atmospheres, found that the best agreement between the observations and the synthetic spectra of Nova LMC 1991 requires a metallicity of Z $= 0.1$ Z$_\odot$. This is a significantly lower metallicity than the canonical LMC value of $\sim$ 1/3 solar and lends stronger support to the identification of the λ313.0 nm feature as ^{7}Be II.

Beryllium and magnesium have similar ionization potentials and a rough estimate of the their relative abundances can be derived from the ratio of the EWs of their resonance absorption doublets. The two lines show a similar velocity profiles at the same blue-shifted velocity, which indicates that the two features are produced under similar conditions. The observed absorption EW of Mg II could be partially reduced by the presence of the emission component. Moreover, lines of singly ionized elements, e.g. Cr II, Ti II and Fe II, contribute for 10–20 per cent to the EW of the λ313.0 line. From the data shown in Fig. 15, we measure an EW ratio of about 4.2/11.5 $= 0.37$ in the LMC1991 nova and a ratio of 3.6/12.9 $= 0.28$ in LMC 1992 nova and we adopt an average ratio $W(313.0)/W(280.0) \sim 0.30$. In the optically thin regime, this ratio provides an estimate of the number of absorbers (N_i) through the common relation of $W \propto N_i \times f_{ij} \times \lambda^2$. Since $f_{ij}(313.0)/f_{ij}(280.0) \sim 0.5$ the observed EW ratio provides $N_i(313.0)/N_i(280.0) = 0.48$ Since the second ionization potentials of the two ions have similar values (i.e. 18.21 eV and 15.04 eV, respectively), similar ionization fractions are expected. Thus, the above derived ratio also provides an estimate of the total ^{7}Be/Mg abundance. Assuming the magnesium abundance being 1/4 of the solar (similar to the value assumed for the SMC, see the next section), namely 9.08×10^{-6} (Lodders 2019), the ^{7}Be II abundance relative to hydrogen is given by N(^{7}Be)/N(H) $= 9.08 \times 10^{-6} \times 0.48 \sim 4.36 \times 10^{-6}$, which is very close to the yields derived here for the novae of the SMC.

5.3 On the Li-enrichment in the SMC

Howk et al. (2012), from the detection of the Li I interstellar line along the line of sight of SK 143, derived N(^{7}Li)/N(H) $= (4.8 \pm 1.8) \times 10^{-10}$ and an absolute Li abundance of A(Li) $= 2.68 \pm 0.16$, a value which is close to the level expected from the SBBN, when considering the CMB baryon density. Howk et al. (2012) concluded that the value measured in the SMC interstellar medium corresponds to the primordial with a negligible stellar post-BBN production.

On the other hand, the nova lithium yield estimated here suggests a non-negligible role of classical novae in the lithium enrichment of the SMC. The ^{7}Be produced in SMC novae will enrich the ISM of the SMC with freshly produced ^{7}Li. The lithium yield inferred from the analysis of ASASSN-19qv and ASASSN-20ni is $M_{^7Li} = M_{^7Be} = (3.7 \pm 0.6) \times 10^{-10}$ M$_\odot$. Assuming all SMC novae eject a similar amount of lithium into the ISM of the SMC, we can have an approximate estimate of their contribution. For this purpose, we need to know the nova rate in the SMC. This quantity was recently discussed by Della Valle & Izzo (2020). These authors found a robust lower limit for the SMC nova rate of 0.7 events per year, which is consistent with $r = 0.9 \pm 0.4$ yr^{-1}, measured by Mróz et al. (2016). In the following, we take the latter value of the rate as a constant over the age of the SMC. The oldest globular cluster (GC) in the SMC, NGC 121, is 2–3 Gyr younger than the oldest GCs in the Milky Way (Glatt et al. 2008), and the average age of stars in the outer regions of the SMC is of $t_{\rm SMC} = 10.6 \pm 0.5$ Gyr (Dolphin et al. 2001). Considering a time delay of $\sim$2 Gyr for the formation of a nova-progenitor WD system, we assume for the action of nova system in the SMC a time interval $\tau = 8.6 \pm 0.5$ Gyr. Thus, the total

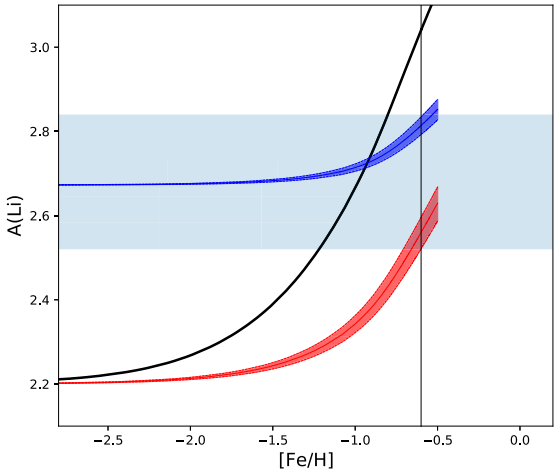

Figure 16. The Li evolution in the SMC assuming the nova yields derived in this paper starting from two different Li initial values: in red the Spite plateau and in blue the CMB + BBN nucleosynthesis. The two curves for each initial lithium abundance and the derived nova yields with their error are shown by shaded regions. The model include astration as well as spallation nucleosynthesis and a modest AGB contribution. The present Li abundance measured in the ISM of SMC derived by Howk et al. (2012) with $\pm 1\sigma$ error is shown with the shaded horizontal band. Finally, the black curve shows the Li evolution derived when a chemical evolution of the SMC but with a Li-yield typical of our Galaxy, namely a factor 4 higher than of the SMC, is considered (Cescutti & Molaro 2019). Note how much the expected value for A(Li) would be off with respect to the present Li abundance value in the SMC if we consider MW-like yields.

lithium production from classical novae amounts to

$$M_{{\rm Li},n} = M_{^7{\rm Li}} \times r \times \tau \quad (2)$$

which gives

$$M_{{\rm Li},n} = (3.7 \pm 0.6) \times 10^{-10} \times 0.9 \times (8.6 \pm 0.5) \times 10^9 = (2.8 \pm 1.9){\rm M}_\odot. \quad (3)$$

The uncertainties reported in the final estimate of $M_{{\rm Li},n}$ correspond to maximum errors.

This value can be compared with Li/H through the SMC mass. An estimate of the neutral hydrogen gas mass is $M_{\rm H\,I} = 4.2 \times 10^8$ M$_\odot$ by means of the H I 21cm line observed with the Australian Telescope Compact Array radio telescope (Stanimirović, Staveley-Smith & Jones 2004). This value is also in agreement with the results from the Parkes H I survey, $M_{\rm H\,I} = 4.02 \pm 0.08 \times 10^8$ M$_\odot$ (Brüns et al. 2005). The additional contribution of the molecular hydrogen H_2 can be derived from the far-infrared maps provided by the *Spitzer* Survey of the SMC. Leroy et al. (2007) estimated a total mass of $M_{H_2} = 3.2 \times 10^7$ M$_\odot$. Adding this value twice to the neutral hydrogen mass, we obtain a final value for the hydrogen mass of $M_{\rm H} = (4.8 \pm 0.2) \times 10^8$ M$_\odot$. The total mass accounting also for stars was estimated by McConnachie (2012) in 9.20×10^8 M$_\odot$. Therefore, the atomic fraction Li/H in the SMC due to novae becomes N(^{7}Li)/N(H) $= (4.0 \pm 1.5) \times 10^{-10}$, or A(Li) $= 2.64$, which suggests that a non-negligible fraction of the lithium observed in the SMC could be originated from classical nova explosions.

In Fig. 16, we present the lithium evolutionary curve for a detailed chemical model for the SMC. The model is similar to those of chemical evolution of dwarf spheroidal galaxies described in Lanfranchi, Matteucci & Cescutti (2006) as well as for the Gaia-Enceladus dwarf galaxy described in Cescutti, Molaro & Fu (2020), the first model following the evolution of lithium in external galaxies

(see also Matteucci et al. 2021 for more satellites of the Milky Way). Compared to our Galaxy, dwarf galaxies have lower star formation efficiencies and galactic winds that prevent to reach solar metallicities. In particular, our model for SMC follows the equations described in Cescutti et al. (2020) and it has an evolution that lasts 10 Gyr, a Gaussian infall law with a peak at 4 Gyr and sigma of 1 Gyr. The total mass surface density is 50 $M_{\odot}$ pc^{-2} with a star formation efficiency of 0.06 Gyr^{-1}. We assume a Galactic wind that starts after 7 Gyr, with a wind efficiency of 0.8 Gyr^{-1}, proportional to the gas still present in the galaxy. These chemical evolution parameters are fixed to reproduce the metallicity distribution function and the [α/Fe] versus [Fe/H] trend observed in giant stars of the SMC by Mucciarelli (2014). For lithium, we consider the same nucleosynthetic channels considered in Cescutti & Molaro (2019). The Li production is mainly from novae, with a small contribution from production from AGB (Ventura & D'Antona 2010). For the spallation production, we adopt the spallation rates which are empirically derived from beryllium observations in stars belonging to the Gaia-Enceladus dwarf galaxy, which, however, remains very similar to that of the Galaxy (Molaro, Cescutti & Fu 2020b). In *Gaia*-Enceladus, the relation is

$$\mathrm{A(Be)} = 0.729(\pm 0.059) \times [\mathrm{Fe/H}] + 0.856(\pm 0.117). \quad (4)$$

The scaling of Li/Be $\approx$ 7.6 for spallation processes is adopted (Molaro et al. 1997) which provides at the SMC metallicity a value of A(Li) = 1.94 made by spallation processes only. The Li destruction due to astration in the stellar recycling is also taken into account. The model is shown for two different initial Li values, according to the SBBN + Planck nucleosynthesis of A(^{7}Li) = 2.72 $\pm$ 0.06 (Cyburt et al. 2016), or the Spite plateau at A(Li) = 2.20 $\pm$ 0.05. The present estimated values are A(Li) = 2.56 $\pm$ 0.04 when starting from the primordial value taken from the halo stars and A(Li)= 2.81 $\pm$ 0.02 for the higher primordial value expected by the SBBN with the baryonic density of the deuterium measurement. These could be compared with the value of A(Li) = 2.68 $\pm$ 0.16 measured by Howk et al. (2012) in the interstellar medium. Unfortunately, the present error bar in the ISM determination is so large that it is not possible to discriminate between the two initial values. If this error can be reduced significantly in future observations then the present abundance could discriminate between the two initial values. If the present Li abundance is at the level of the SBBN-Planck Li value this would require a low primordial value in order to account for the stellar Li production. On the contrary, if the primordial Li value is what was indicated by the SBBN and Planck, then the Li today in the SMC needs to be slightly higher than that due to the contribution of the stellar Li synthesis. At face value the Howk et al. (2012) measurement of A(Li) = 2.68 $\pm$ 0.16 favours a low primordial value.

6 CONCLUSIONS

After the discovery of ASASSN-19qv in the SMC, we were granted a DDT programme at ESO-VLT with the high-resolution spectrographs UVES and X-shooter, in order to study the spectroscopic evolution of ASASSN-19qv and to search for the ^{7}Be isotope in the early epochs of the nova outburst. One year later, and in the middle of the pandemic, we used granted telescope time to observe the outburst of another nova in the SMC, ASASSN20-ni. The target-of-opportunity nature of our program allowed us to observe the nova very soon after its discovery and the first high-resolution spectrum with VLT/UVES was obtained 4 d later. We summarize the main results here:

(i) The ^{7}Be II resonance transitions were detected in ASASSN-19qv at two distinct epochs, and also in ASASSN-20ni in all the epochs of the observations.

(ii) We have analysed the outburst spectra in order to infer the amount of ^{7}Be, and therefore ^{7}Li, synthesised in TNR of both novae. This provided the first estimate of the lithium yield by novae in the SMC, namely N(^{7}Li)/N(H) = (5.3 $\pm$ 0.2) $\times$ 10^{-6}. With a conservative value of $M_{\mathrm{H,ej}} = 10^{-5}$ $M_{\odot}$ we have $M_{^7\mathrm{Be}} = (3.7 \pm 0.6) \times 10^{-10}$ $M_{\odot}$ per nova event.

(iii) We have also studied two historical novae exploded in the LMC which have been followed by the *IUE* satellite. The *IUE* LWP spectra of LMC 1991 and LMC 1992 exhibit a strong absorption feature that can be identified as the resonance doublet of singly-ionized ^{7}Be II. The low metallicity of the LMC make less likely to explain the feature as a blend of absorption lines of singly ionized metals. By using Mg as a reference element we obtain a ^{7}Be II abundance of $N(^7Be)/N(H) \sim 4.36 \times 10^{-6}$, which, despite several uncertainties, is very close to that derived for the novae of the SMC. To note that Mg and ^{7}Be II have similar second ionization potentials and of therefore the ^{7}Be II yields obtained by using Mg are quite insensitive to the presence of overionization effects in the ejecta.

(iv) When these yields are inserted in a chemical evolution model suited for the SMC they result into a present Li abundance of the order of A(Li) = 2.56 when starting form a low primordial ^{7}Li value or A(Li) = 2.8 when starting from a high primordial value. The observation of present Li in the interstellar gas of the SMC of Howk et al. (2012) of A(Li) = 2.68 $\pm$ 0.16 are consistent with both values within 1 σ error and precludes from any firm conclusion.

(v) The evidence of ^{7}Be in the CN ejecta observed in the Magellanic Clouds suggests that the thermonuclear reactions giving origin to this isotope during the TNR is effective also in environments characterized by a general sub-solar metallicity, as it is indeed the case for the two main Milky Way satellites. All recent CN explosion simulations have always considered a solar abundance value for the material accreted on to the primary WD in a CN binary system (Casanova, José & Shore 2018; José, Shore & Casanova 2020; Starrfield et al. 2020). Therefore, our result implies the necessity of further simulations, characterized by a sub-Solar metallicity for the matter accreting the primary WD, that can support our finding.

(vi) This result implies that CNe are likely the main lithium factories also in systems external to our Galaxy. Further observations will constrain much better the lithium yield in nearby galaxies, such as the SMC and the LMC. This goal will be easily reachable with the possibility to use advanced high-resolution spectrographs observing the near-UV range such as the proposed CUBES at ESO/VLT (Ernandes et al. 2020).

ACKNOWLEDGEMENTS

We are very grateful to the several dozens of observers worldwide who have contributed with their observations to the AAVSO International Database, a resource that we always consider as a main reference for classical novae evolution light curves. This paper includes data collected with the TESS mission, obtained from the MAST data archive at the Space Telescope Science Institute (STScI). Funding for the TESS mission is provided by the NASA Explorer Program. STScI is operated by the Association of Universities for Research in Astronomy, Inc., under NASA contract NAS 5–26555. We are also grateful to the ESO director for the DDT programme 2103.D-5044. LI was supported by grants from VILLUM FONDEN (project number 16599 and 25501). AA is supported by a Villum

Experiment Grant (project number 36225). This work was partially supported by the European Union (ChETEC-INFRA, project no. 101008324 and ChETEC, CA16117). EA acknowledges NSF award AST-1751874, NASA award 11-Fermi 80NSSC18K1746, NASA award 16-Swift 80NSSC21K0173, and a Cottrell fellowship of the Research Corporation. M.H. acknowledges support from grant PID2019-108709GB-I00 from MICINN (Spain). We acknowledge Lucas Macri, Jay Strader, and Laura Chomiuk for help with obtaining and reducing the SOAR spectrum. We have also made an extensive use of PYTHON scripts, developed specifically for the analysis of this nova, as well as of IRAF tools for a counter-check of all the measurements presented in this work. We recognize the use of the *NUMPY* (Van Der Walt, Colbert & Varoquaux 2011), *MATPLOTLIB* (Hunter 2007), and the *ASTROPY* (Astropy Collaboration et al. 2013) python packages. Last, but not least, LI is also very grateful to Anna Serena Esposito, given that the first evidence of ^{7}Be from a SMC nova was found the same day of our wedding: LI fully recognizes her patience in tolerating the time spent on activating, reducing and analysing the data within the most beautiful days of our life together.

DATA AVAILABILITY

The data underlying this article will be shared on reasonable request to the corresponding author.

REFERENCES

Andrea J., Drechsel H., Starrfield S., 1994, A&A, 291, 869
Astropy Collaboration et al., 2013, A&A, 558, A33
Aydi E. et al., 2019, Astron. Tel., 12907, 1
Aydi E. et al., 2020, Astron. Tel., 14123, 1
Aydi E., Buckley D. A. H., Mohamed S., Whitelock P. A., 2018, Astron. Telegram, 11287, 1
Bode M. F., Evans A., 2012, Classical Novae, Cambridge University Press, Cambridge
Boggess A. et al., 1978, Nature, 275, 372
Bohlsen T. C., 2019a, Astron. Telegram, 12917, 1
Bohlsen T. C., 2019b, Astron. Telegram, 12938, 1
Bonifacio P. et al., 2015, A&A, 579, A28
Bouret J. C., Lanz T., Hillier D. J., Heap S. R., Hubeny I., Lennon D. J., Smith L. J., Evans C. J., 2003, ApJ, 595, 1182
Brüns C. et al., 2005, A&A, 432, 45
Bucciarelli B. et al., 2008, in Jin W. J., Platais I., Perryman M. A. C., eds, IAU Symp. Vol. 248, A Giant Step: from Milli- to Micro-arcsecond Astrometry. Kluwer, Dordrecht, p. 316
Cameron A. G. W., 1955, ApJ, 121, 144
Cameron A. G. W., Fowler W. A., 1971, ApJ, 164, 111
Carrera R., Gallart C., Aparicio A., Costa E., Méndez R. A., Noël N. E. D., 2008, AJ, 136, 1039
Casanova J., José J., Shore S. N., 2018, A&A, 619, A121
Cassatella A., Altamore A., González-Riestra R., 2002, A&A, 384, 1023
Cescutti G., Molaro P., 2019, MNRAS, 482, 4372
Cescutti G., Molaro P., Fu X., 2020, Mem. Soc. Astron. Italiana, 91, 153
Choudhury S., Subramaniam A., Cole A. A., Sohn Y. J., 2018, MNRAS, 475, 4279
Christian G. et al., 2018, Phys. Rev. C, 97, 025802
Chugai N. N., Kudryashov A. D., 2020, preprint (arXiv:2007.07044)
Cioni M. R. et al., 2011, Messenger, 144, 25
Coc A., Uzan J.-P., Vangioni E., 2014, J. Cosmol. Astropart. Phys., 10, 50
Cyburt R. H., Fields B. D., Olive K. A., Yeh T.-H., 2016, Rev. Modern Phys., 88, 015004
D'Antona F., Matteucci F., 1991, A&A, 248, 62
Della Valle M., Izzo L., 2020, A&AR, 28, 3
Dolphin A. E., Walker A. R., Hodge P. W., Mateo M., Olszewski E. W., Schommer R. A., Suntzeff N. B., 2001, ApJ, 562, 303
Ernandes H. et al., 2020, in Evans C. J., Bryant J. J., Motohara K., eds, SPIE Conf. Ser. SPIE,Bellingham, WA, p. 1144760
Ferland G. J. et al., 2017, RMxAA, 53, 385
Fields B. D., 2011, Ann. Rev. Nucl. Part. Sci., 61, 47
Fields B. D., Molaro P., Sarkar S., 2014, Chin. Phys. C, 38, preprint (arXiv:1412.1408)
Fu X. et al., 2018, A&A, 610, A38
Fu X., Bressan A., Molaro P., Marigo P., 2015, MNRAS, 452, 3256
Gallagher J. S., Starrfield S., 1978, ARA&A, 16, 171
Gehrz R. D., Truran J. W., Williams R. E., Starrfield S., 1998, PASP, 110, 3
Glatt K. et al., 2008, AJ, 135, 1106
Grisoni V., Matteucci F., Romano D., Fu X., 2019, MNRAS, 489, 3539
Howk J. C., Lehner N., Fields B. D., Mathews G. J., 2012, Nature, 489, 121
Hunter J. D., 2007, Comput. Sci. Eng., 9, 90
Izzo L. et al., 2015, ApJ, 808, L14
Izzo L. et al., 2018, MNRAS, 478, 1601
José J., Shore S. N., Casanova J., 2020, A&A, 634, A5
Kafka S., 2021, https://www.aavso.org
Kastner S. O., Bhatia A. K., 1995, ApJ, 439, 346
Kochanek C. S., 2017, PASP, 29, 104502
Korn A. J., Becker S. R., Gummersbach C. A., Wolf B., 2000, A&A, 353, 655
Lambert D. L., Reddy B. E., 2004, MNRAS, 349, 757
Lanfranchi G. A., Matteucci F., Cescutti G., 2006, MNRAS, 365, 477
Lawler J. E., Sneden C., Nave G., Den Hartog E. A., Emrahoğlu N., Cowan J. J., 2017, ApJS, 228, 10
Leroy A., Bolatto A., Stanimirovic S., Mizuno N., Israel F., Bot C., 2007, ApJ, 658, 1027
Lodders K., 2019, preprint (arXiv:1912.00844)
Lodders K., Palme H., Gail H.-P., 2009, Solar System, Landolt-Börnstein - Group VI Astronomy and Astrophysics, Vol. 4B. Springer, Berlin, p. 712
Madden S. C. et al., 2013, PASP, 125, 600
Matteucci F., 2021, A&A Rev., 29, 5
Matteucci F., Molero M., Aguado D. S., Romano D., 2021, MNRAS, 505, 200
McConnachie A. W., 2012, AJ, 144, 4
Molaro P. et al., 2022, MNRAS, 509, 3258
Molaro P., Bonifacio P., Castelli F., Pasquini L., 1997, A&A, 319, 593
Molaro P., Cescutti G., Fu X., 2020b, MNRAS, 496, 2902
Molaro P., Izzo L., Bonifacio P., Hernanz M., Selvelli P., della Valle M., 2020a, MNRAS, 492, 4975
Molaro P., Izzo L., Mason E., Bonifacio P., Della Valle M., 2016, MNRAS, 463, L117
Mróz P. et al., 2016, ApJS, 222, 9
Mucciarelli A., 2014, Astron. Nachr., 335, 79
Mukai K., Sokoloski J. L., 2019, Phys. Today, 72, 38
Nidever D. L. et al., 2017, AJ, 154, 199
Payne-Gaposchkin C. H., 1964, The Galactic Novae. Dover Publication, New York
Planck Collaboration et al., 2016, A&A, 594, A13
Prantzos N., 2012, A&A, 542, A67
Ramírez I., Fish J. R., Lambert D. L., Allende Prieto C., 2012, ApJ, 756, 46
Romano D., Matteucci F., Molaro P., Bonifacio P., 1999, A&A, 352, 117
Sbordone L. et al., 2010, A&A, 522, A26
Schwarz G. J., Shore S. N., Starrfield S., Hauschildt P. H., Della Valle M., Baron E., 2001, MNRAS, 320, 103
Selvelli P., Molaro P., Izzo L., 2018, MNRAS, 481, 2261
Setoodehnia K., Marshall C., Kelley J. H., Liang J., Portillo Chaves F., Longland R., 2018, Phys. Rev. C, 98, 055804
Shappee B. J. et al., 2014, ApJ, 788, 48
Spite F., 1990, Mem. Soc. Astron. Italiana, 61, 663
Spite F., Spite M., 1982, A&A, 115, 357
Spitzer L., 1998, Physical Processes in the Interstellar Medium. Wiley-VCH
Stanimirović S., Staveley-Smith L., Jones P. A., 2004, ApJ, 604, 176
Starrfield S., Bose M., Iliadis C., Hix W. R., Woodward C. E., Wagner R. M., 2020, ApJ, 895, 70
Starrfield S., Truran J. W., Sparks W. M., Arnould M., 1978, ApJ, 222, 600

Tajitsu A., Sadakane K., Naito H., Arai A., Aoki W., 2015, Nature, 518, 381
Tajitsu A., Sadakane K., Naito H., Arai A., Kawakita H., Aoki W., 2016, ApJ, 818, 191
Trundle C., Dufton P. L., Hunter I., Evans C. J., Lennon D. J., Smartt S. J., Ryans R. S. I., 2007, A&A, 471, 625
Van Der Walt S., Colbert S. C., Varoquaux G., 2011, Computing in Science & Engineering, 13, 22
Ventura P., D'Antona F., 2010, MNRAS, 402, L72
Warner B., 1989, in Classical Novae. Cambridge University Press, Cambridge, p. 1
Way Z. et al., 2020, Astron. Telegram, 14122, 1
Williams R. E., 1994, ApJ, 426, 279
Williams R. E., Hamuy M., Phillips M. M., Heathcote S. R., Wells L., Navarrete M., 1991, ApJ, 376, 721
Williams R., 2012, AJ, 144, 98
Williams R., Mason E., Della Valle M., Ederoclite A., 2008, ApJ, 685, 451

This paper has been typeset from a TEX/LATEX file prepared by the author.